



ELSEVIER

Deep-Sea Research II 51 (2004) 1129–1149

DEEP-SEA RESEARCH  
PART II

[www.elsevier.com/locate/dsr2](http://www.elsevier.com/locate/dsr2)

# Spatial and temporal characteristics of sediment plumes and phytoplankton blooms in the Santa Barbara Channel

M.P. Otero\*, D.A. Siegel

*Institute for Computational Earth System Science, University of California, Santa Barbara, CA 93106-3060, USA*

Received 28 October 2002; accepted 15 April 2004

Available online 3 September 2004

## Abstract

Satellite ocean-color and sea-surface temperature (SST) imagery are used to assess the occurrence, extent and duration of surface sediment plumes from discharged stormwaters and phytoplankton blooms in the Santa Barbara Channel (SBC), California. Nearly four years (October 1997–June 2001) of Advanced Very High Resolution Radiometer and Sea-viewing Wide Field-of-view Sensor local area coverage imagery, in situ measurements, and supporting data are analyzed. Monthly mean annual cycles of SST, chlorophyll (Chl) and the water-leaving radiance at 555 nm ( $L_{wN}(555)$ ), an index for sediment-affected waters, show plumes associated with runoff in winter, while blooms occur in the late spring–early summer and are associated with cool SST and upwelling favorable winds. Interannual variations are consistent with remote forcing by El Niño cycles. During the 1997–1998 El Niño, Chl concentrations are moderate, and El Niño-induced floodwater discharges result in high  $L_{wN}(555)$  values throughout the SBC. However, a correspondence between El Niño–La Niña state and Chl is not found for the SBC due to what appears to be the advection of nutrient-depleted waters from the east. Empirical plume and bloom indices show that plumes occur episodically in response to discharge events whereas blooms occur more regularly and can cover up to 95% of the SBC. Empirical orthogonal function analysis is used to spatially and temporally deconvolve processes regulating SST, Chl and  $L_{wN}(555)$ . The first Chl mode contains 43% of the temporal variance and is associated with wind-driven upwelling in spring and summer. The first  $L_{wN}(555)$  mode contains 51% of the temporal variance and is associated with episodic terrestrial runoff events in February and March. The second modes for both Chl and  $L_{wN}(555)$  represent the transition from runoff-dominated processes in winter to upwelling and bloom-dominated processes in summer.

© 2004 Elsevier Ltd. All rights reserved.

## 1. Introduction

Accelerated anthropogenic pressures on the world's continental margins demand an improved understanding of the coastal environment in order to ensure its economic and ecological viability in the future. Coastal circulations are inherently

\*Corresponding author. Now at Scripps Institution of Oceanography, University of California, San Diego, La Jolla, CA 92093-0213, USA.

E-mail address: [motero@mpl.ucsd.edu](mailto:motero@mpl.ucsd.edu) (M.P. Otero).

complicated as terrestrial boundaries and bathymetric variations play a large role in the dynamics. Terrestrial runoff also may be an important source of freshwater, sediments, nutrients and potential pollutants for the coastal ocean. In the past, severe undersampling coupled with high spatial and temporal variability limited our knowledge of the coastal ocean. Synoptic views obtained by satellite remote sensing have the potential for improving our understanding of nearshore processes at a variety of space and timescales (e.g., IOCCG, 2000).

The Santa Barbara Channel (SBC) is located along the northernmost edge of the Southern California Bight. The northern border of the SBC is comprised of an east–west trending section of the California coast while the southern border is made up of the Northern Channel Islands: San Miguel, Santa Rosa, Santa Cruz and Anacapa Islands (Fig. 1). The passageways between the four islands are relatively narrow and shallow compared with the eastern and western borders of the SBC. The Santa Clara River is the largest

watershed draining into the SBC (Fig. 1), although it is clearly not the only terrestrial source for the SBC (Mertes and Warrick, 2001).

The oceanographic setting of the SBC is controlled by several forces that interact with its unique geography. First, the SBC is embedded within the California Current System comprised of the equatorward flowing California Current and the recirculating Southern California Eddy and Inshore Countercurrent (Hickey, 1979; Lynn and Simpson, 1987). The California Current carries relatively cool, fresh waters equatorward offshore of the SBC's western margin while the Inshore Countercurrent and the Southern California Eddy bring warmer, more saline waters to the SBC. Seasonally, the California Current intensifies during the spring in response to large-scale, upwelling favorable winds along the west coast of the US (Lynn and Simpson, 1987). When the California Current relaxes, poleward flows are observed nearshore within the Southern California Bight (Hickey, 1979).

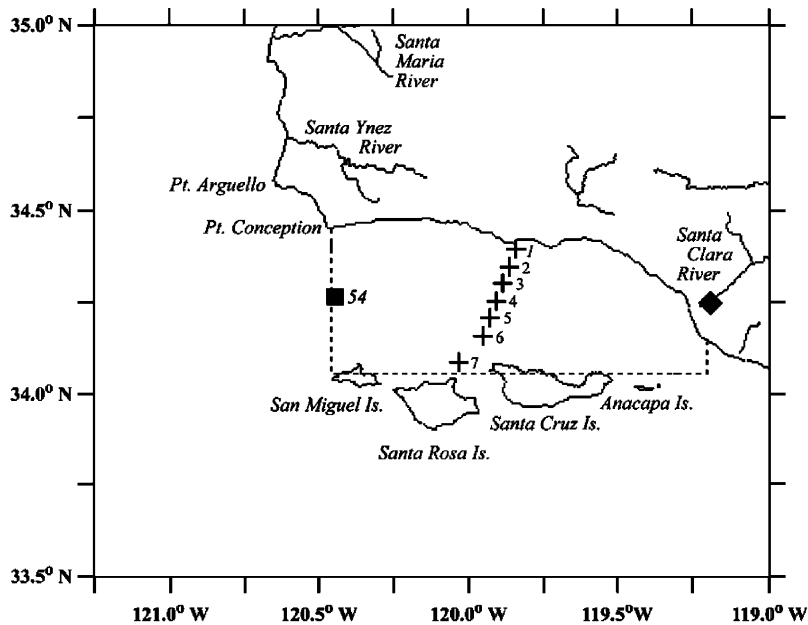


Fig. 1. Map indicating sampling sites and major geographic reference points around the SBC region. The square indicates the location of NDBC buoy 46054, the diamond indicates the USGS gauge site used for measuring discharge from the Santa Clara River and plus signs numbered 1–7 indicate PnB sampling locations. The dotted line circumscribes the area used for making regional averages of the SBC from satellite data.

Second, the large-scale wind field is driven by the relative strength of the North Pacific High over the subtropical Pacific Ocean (Reid et al., 1958). During fall and winter, the North Pacific High is relatively weak and the passage of mid-latitude storms dominate wind climate. However, during the spring, strong, persistent equatorward winds occur along the US west coast continuing through the summer. At Point Conception, strong wind gradients occur as the equatorward winds detach from the coast (Winant and Dorman, 1997). The SBC lies in the transition between strong winds to the north and sheltered waters to the south. In the eastern portion of the SBC, wind speeds are much lower, resulting in a large and persistent wind stress curl over the SBC (Dorman and Winant, 2000; Oey et al., 2001).

Circulation patterns within the SBC itself result from wind forcing on local and large-scales as well as the along-channel pressure gradients created by the California Current System (Brink et al., 1984; Harms and Winant, 1998; Hickey et al., 2003). Analysis of surface current observations shows the presence of three primary synoptic circulation states within the SBC (Winant et al., 2003). These synoptic flow states show spatial current patterns resulting from local wind forcing and the along-channel pressure gradient.

The location, timing and intensity of phytoplankton blooms respond to variations in horizontal and vertical circulations. Rates of primary productivity are limited by the flux of nutrients, primarily nitrate concentrations, to the euphotic zone (Eppley et al., 1979). The major nutrient supply is created by coastal upwelling primarily in western portion of the SBC (Atkinson et al., 1986; Hayward and Venrick, 1998). These upwelled waters from near Point Conception typically flow south and often enter the SBC (Jones et al., 1988). The resulting chlorophyll (Chl) biomass is concentrated in the upper 25 m of the water column and subsurface maxima are rarely observed (Venrick, 1998). Temporal fluctuations of mixed-layer Chl within the SBC are well correlated with nearby stations outside of the channel (Hayward and Venrick, 1998), indicating that biological processes within the SBC are regulated, in part, by Bight-scale processes.

Climate in the SBC region is characterized by short, wet winters and long, dry summers, which has an important influence on the terrestrial input of suspended sediments (Milliman and Syvitski, 1992). Significant streamflow occurs during and just after storms while major storms mobilize sediments accumulated in stream channels seaward (Scott and Williams, 1978; Milliman and Syvitski, 1992). The Santa Clara River is the largest watershed draining into the SBC (Fig. 1). The numerous mountainous watersheds of the Transverse Range have the highest sediment yields within Southern California due to the steep watersheds, tectonic setting, sediment erodibility, and their susceptibility to flooding (Milliman and Syvitski, 1992; Inman and Jenkins, 1999; Mertes and Warrick, 2001).

The offshore extent of sediment plumes entering the SBC appears to be driven primarily by the size of the watershed and strength of the storm whereas the nature of terrestrial and nearshore geologic and geographic features appear to be second order (Mertes and Warrick, 2001; Warrick, 2002). Although these offshore suspended sediment plumes account for less than 2% of the total suspended sediment output from their coastal watersheds (Mertes and Warrick, 2001), they delineate regions affected by stormwater runoff. There also is a great deal of interannual variability in precipitation and streamflow, some of which is associated with El Niño events although a robust local relationship between El Niño and precipitation has not been found (Haston and Michaelsen, 1994). During February 1998, extreme flooding occurred throughout California coincident with the 1997–1998 El Niño event.

In this paper, satellite imagery from the Sea-viewing Wide Field-of-view Sensor (SeaWiFS) and Advanced Very High Resolution Radiometer (AVHRR) are used to determine the space and time characteristics of sediment plumes and phytoplankton blooms in the SBC. Characteristics of sediment plumes and/or phytoplankton blooms for this region have been evaluated using optical means from in situ observations (Mitchell and Kahru, 1998; Toole and Siegel, 2001) or from satellite orbit (Smith et al., 1998; Kahru and Mitchell, 1999; Mertes and Warrick, 2001;

Warrick et al., 2004). Here, we use local area coverage imagery of sea-surface temperature (SST), Chl concentration and the normalized water-leaving radiance at 555 nm ( $L_{wN}(555)$ ) to assess the effects of upwelling and terrestrial runoff processes. Example images typifying the spatial patterns associated with upwelling and terrestrial runoff events are followed by monthly mean annual cycles that show the seasonal evolution of salient features in the SBC. Forcing of the system is assessed using time-series of local wind stress, discharge records for nearby watersheds, and the southern oscillation index (SOI). Indices for detecting sediment plumes and phytoplankton blooms are developed and applied to describe the extent, duration and frequency of these events. Finally, upwelling and runoff processes are temporally and spatially resolved from one another in both Chl and  $L_{wN}(555)$  fields using empirical orthogonal function (EOF) analysis.

## 2. Data and methods

### 2.1. Field observations from Plumes and Blooms

The Plumes and Blooms (PnB) Project, started in August 1996, provides a means for development and validation of ocean-color algorithms in Case II waters. The PnB field program consists of approximately twice monthly sampling of seven stations across the SBC (+’s in Fig. 1). Field observations of Chl, SST and water-leaving radiance are used to validate SeaWiFS and AVHRR products presented here. All sampling and analysis protocols follow established procedures. Further details regarding the PnB program and methodologies can be found in Toole et al. (2000), Toole and Siegel (2001) and the PnB home page; [www.icess.ucsb.edu/PnB/PnB.html](http://www.icess.ucsb.edu/PnB/PnB.html).

### 2.2. AVHRR SST imagery and its validation

AVHRR imagery were acquired and processed at the Institute for Computational Earth System Science (ICESS), University of California at Santa Barbara (UCSB) ([www.icess.ucsb.edu/avhrr/avhrr.html](http://www.icess.ucsb.edu/avhrr/avhrr.html)). AVHRR images are processed to

Table 1

Summary statistics from comparisons between PnB and satellite data

Sensor	Parameter	Algorithm	$n$	$r^2$
AVHRR	SST	MCSST	367	0.88
SeaWiFS	Chl	OC4v4	154	0.53
SeaWiFS	$L_{wN}(412)$	Reprocessing #3	100	0.07
SeaWiFS	$L_{wN}(443)$	Reprocessing #3	124	0.12
SeaWiFS	$L_{wN}(490)$	Reprocessing #3	128	0.34
SeaWiFS	$L_{wN}(510)$	Reprocessing #3	131	0.26
SeaWiFS	$L_{wN}(555)$	Reprocessing #3	131	0.42
SeaWiFS	$L_{wN}(670)$	Reprocessing #3	108	0.08

SST values using the multi-channel sea-surface temperature (MCSST) algorithm (McClain et al., 1985). Each image was edited by hand to remove residual clouds and five-day composites are computed on a 1-km basis for the Southern California Bight. On average, composite images cover 90.4% of the SBC. Match-up analyses show excellent agreement between satellite-derived and field-observed SST, where the squared correlation coefficient between MCSST and observed SST is 0.88 ( $N = 367$ , Table 1; Otero, 2002). Root mean square deviation between MCSST and observed SST is 0.96 °C, and the mean deviation is -0.41 °C. This indicates a good correspondence between satellite and field-observed quantities. These results support quantitative applications of AVHRR five-day composites in the SBC region.

### 2.3. SeaWiFS ocean-color imagery and its validation

All Level 1A SeaWiFS data with at least partial cloud-free views of the SBC are used in this study. SeaWiFS imagery are processed to Level 2 (Chl and water-leaving radiance spectra) using the SeaWiFS Data Analysis System (version 4.0; <http://seadas.gsfc.nasa.gov>) using default settings of the msl12 command and real-time ancillary data (reprocessing # 3). Scenes with obvious problems, such as cloud-edge effects and low viewing angles, were not analyzed. The data set spans from October 1997 to June 2001.

Statistical comparisons between simultaneous SeaWiFS and in situ observations of the normalized

water-leaving radiance spectra,  $L_{wN}(\lambda)$ , show their best results for the 555 nm band ( $r^2 = 0.42$ ), with a clear deterioration in the relationship for the shorter wavelengths (Table 1). This indicates an overcorrection due to satellite calibration and atmospheric correction algorithm issues (see also Kahru and Mitchell, 1999), and little improvement was found using data from SeaWiFS reprocessing #4 (unpublished results, 2003). SeaWiFS estimates of  $L_{wN}(\lambda)$  are still qualitatively useful. For example, comparison of the spatial and temporal patterns between field-observed and SeaWiFS  $L_{wN}(555)$  measurements show good qualitative agreement where all the major features (mostly due to sediment plumes) are well represented in both data sets (Otero, 2002). Particulate lithogenic silica concentrations are found to be a good indicator of suspended sediment concentrations (Shipe et al., 2002; Warrick 2002). Elevated concentrations of lithogenic silica also are well correlated with determinations of  $L_{wN}(555)$  ( $r^2 = 0.58$ ,  $N = 195$ ; Toole and Siegel, 2001) indicating that  $L_{wN}(555)$  should be a good proxy for suspended sediments.

The SeaWiFS Chl algorithm (OC4v4) provides reasonable Chl retrievals for this region ( $r^2 = 0.53$ ;  $N = 154$ ). This is because errors in water-leaving radiance retrievals effectively cancel out when ratios are calculated (O'Reilly et al., 1998). Spatial-temporal patterns are similar for SeaWiFS and field Chl observations (Otero, 2002). In particular, all major bloom events observed in the field data set are detected using SeaWiFS but with higher temporal and spatial resolution. Most of the blooms also are associated with cool upwelled waters as observed in AVHRR SST imagery; however, apparent blooms are found associated with obvious stormwater conditions (see below). Field observations show that the OC4v4 Chl algorithm performs poorly in offshore sediment plumes from the Santa Clara River ( $r^2 = 0.02$ ,  $N = 9$ , Toole and Siegel, 2001). Under these turbid ocean conditions, the OC4v4 algorithm seems to overestimate Chl retrievals. This caveat aside, the reasonable match-up comparisons with the PnB data set and its space/time consistency justifies using SeaWiFS Chl estimates

as an approximate index of phytoplankton blooms for this region.

SeaWiFS images over the SBC are available at least every other day; however, cloudy and/or foggy conditions result in patchy spatial coverage and temporal gaps of up to 16 days. Monthly composites of Chl and  $L_{wN}(555)$  are computed using maximum likelihood estimators (Campbell et al., 1995) in order to provide appropriate spatial coverage for the statistical analyses that follow. Monthly composites for Chl and  $L_{wN}(555)$  cover nearly all of the SBC (coverage averages 99.2%).

#### 2.4. Environmental forcing indices

Indices of relevant environmental factors are compared with the imagery data sets. First, wind stress estimates from the west channel buoy (NDBC 46054; Fig. 1) are used as an index for the strength of upwelling. Data from June 1996 to June 2001 are used, and wind stress is calculated following Large and Pond (1981). The principal mean wind direction for this site is ESE (toward  $122^\circ$  from north). Discharge records from the Santa Clara River are used as an indicator for terrestrial runoff events as it is the dominant freshwater and sediment source for the SBC and its discharge records are well correlated with those for many other nearby rivers (Warrick, 2002). Daily measurements of streamflow are taken 7 km up from the mouth of the Santa Clara River (USGS gage station 11114000; Fig. 1). Last, the SOI is used as an indicator of El Niño and La Niña conditions, where negative values are indicative of El Niño conditions.

### 3. Results and interpretations

#### 3.1. Examples of episodic events

Individual scenes typifying upwelling and runoff events show small-scale variability otherwise lost in mean states. Paired images of SST and Chl show typical upwelling conditions from April 18, 1998 (Fig. 2). Daily mean wind stress is large ( $0.23 \text{ N m}^{-2}$ ) for this day and directed along its principal axis (toward ESE). Cool waters of

$\sim 11^\circ\text{C}$  are observed along the northwestern shore of the SBC, around Point Conception, Point Arguello and northward. Water upwelled from as far north as Point Arguello appears to advect southeastward into the SBC where it mixes with warmer surrounding waters. Elevated Chl retrievals generally correspond with cooler SST values (Fig. 2). Where SST values vary from 11 to  $13^\circ\text{C}$ , Chl concentrations range from 2 to  $10\text{ mg m}^{-3}$ . Conversely, low Chl values are found coincident with high SSTs. However, along the eastern shore of the SBC, this inverse relationship breaks down. 1998 was an exceptionally wet year (see below),

and nutrient inputs from stormwater may contribute to the elevated Chl values. There also is a clear difference in the Chl–SST relationship found for waters found in the SW and SE quadrants of Fig. 2, where the same SST levels have a lower Chl response offshore (SW quadrant) compared with the inshore station (SE quadrant).

The extent of riverine discharges during flood events also can be assessed using ocean-color imagery. Paired  $L_{\text{WN}}(555)$  and Chl imagery from February 15, 1998, following the second largest discharge event of the time-series, show extremely high  $L_{\text{WN}}(555)$  values associated with sediment

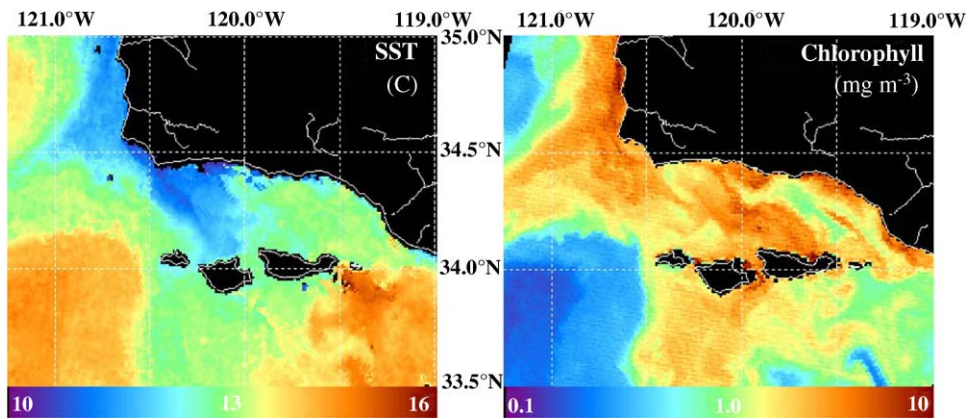


Fig. 2. Paired SST and Chl images during an upwelling event on April 18, 1998. The SST image is a single-day composite of four passes throughout the day.

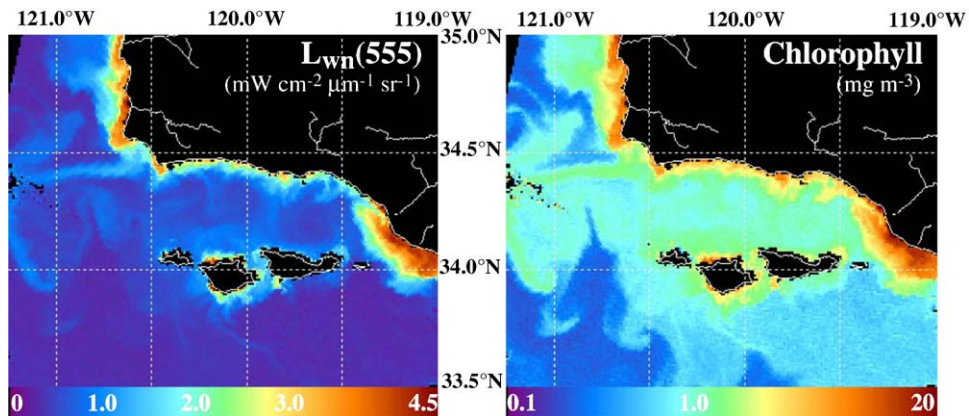


Fig. 3. Paired  $L_{\text{WN}}(555)$  and Chl images during a terrestrial runoff event on February 15, 1998.

plumes (Fig. 3). Peak Santa Clara River discharge ( $991 \text{ m}^3 \text{ s}^{-1}$ ) occurred on February 6, 1998.  $L_{\text{wN}}(555)$  values exceed  $2.0 \text{ mW cm}^{-2} \mu\text{m}^{-1} \text{ sr}^{-1}$  within plume regions, similar to field observations within the Santa Clara River plume (Toole and Siegel, 2001). Chl retrievals in the plume reach  $20 \text{ mg m}^{-3}$ , suggesting that blooms are induced by runoff. However, Chl estimates may not be valid within the discharge plume. The plume emanating from the Santa Clara River extends across and out of the eastern mouth of the SBC, while a filament flows westward off Point Conception and bifurcates offshore (Fig. 3). Elevated values of  $L_{\text{wN}}(555)$  are found along the entire coast, with the largest plumes found near river mouths. The Santa Clara River plume appears to be advected equatorward consistent with local current measurements at this time (Warrick et al., 2004). Sediment plumes circling Santa Rosa Island are larger than those around other Channel Islands due to its radial discharge and shallow surrounding bathymetry (Mertes et al., 1998).

### 3.2. A regional satellite climatology of the Santa Barbara Channel

Monthly mean distributions show the seasonal evolution of SST, Chl and  $L_{\text{wN}}(555)$  for the SBC (Figs. 4–6). Region-wide seasonal warming reaches a maximum in fall, while the coolest SST values are found in spring. The along-channel temperature gradient peaks in early summer as warm Southern California Bight waters are advected into the SBC where they meet cool upwelled waters in the west. Maximum poleward flow within the Bight occurs in summer (Lynn and Simpson, 1987), which combined with seasonal warming, results in the warm SST values from July to October.

Chl patterns generally show an inverse relationship with SST (Figs. 3 and 4) where the highest Chl levels occur in the spring and are associated with low SST values due to upwelling. Monthly mean Chl values peak at  $\sim 3 \text{ mg m}^{-3}$  during April and May within the channel north of Santa Rosa Island and correspond to the lowest SST values

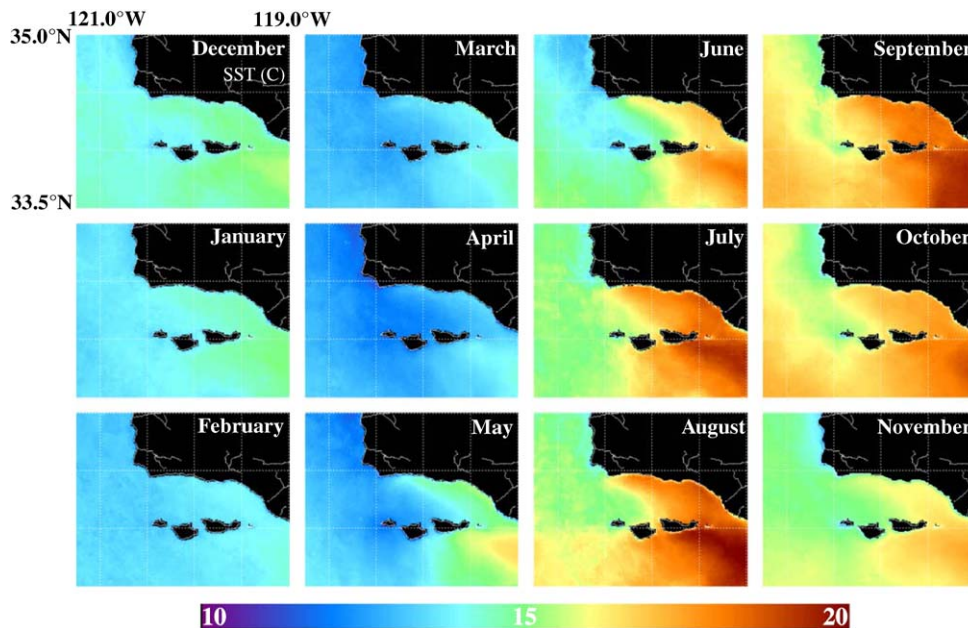


Fig. 4. SST monthly mean annual cycle computed from the AVHRR five-day composite data set. Images above are composites of all data from each month. The monthly mean annual cycle is computed from data between October 1997 and June 2001 for consistency with SeaWiFS data availability.

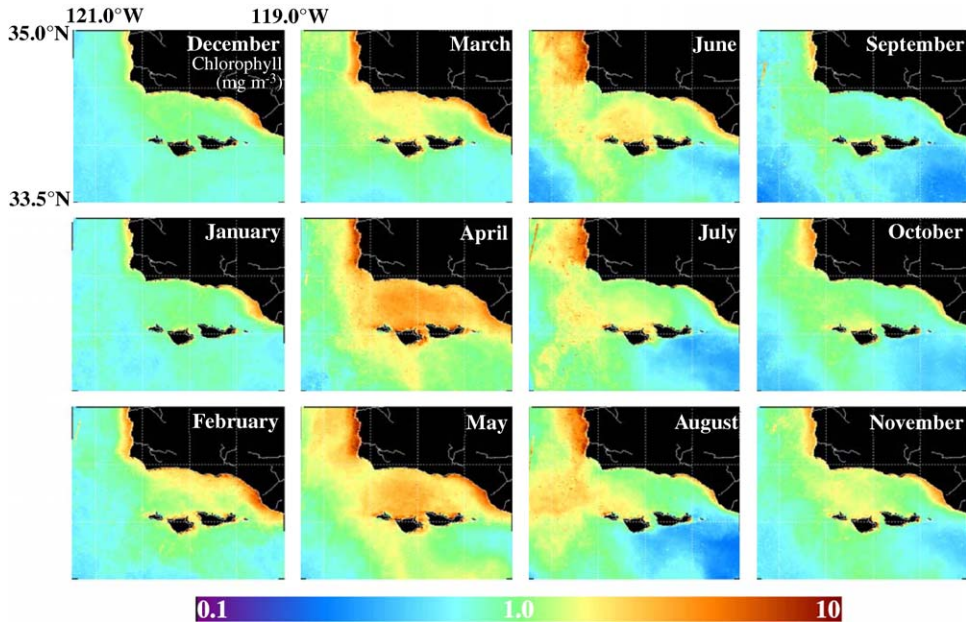


Fig. 5. Chl monthly mean annual cycle computed from all available images. Images above are composites of all data from each month. The monthly mean annual cycle is computed from October 1997 to June 2001.

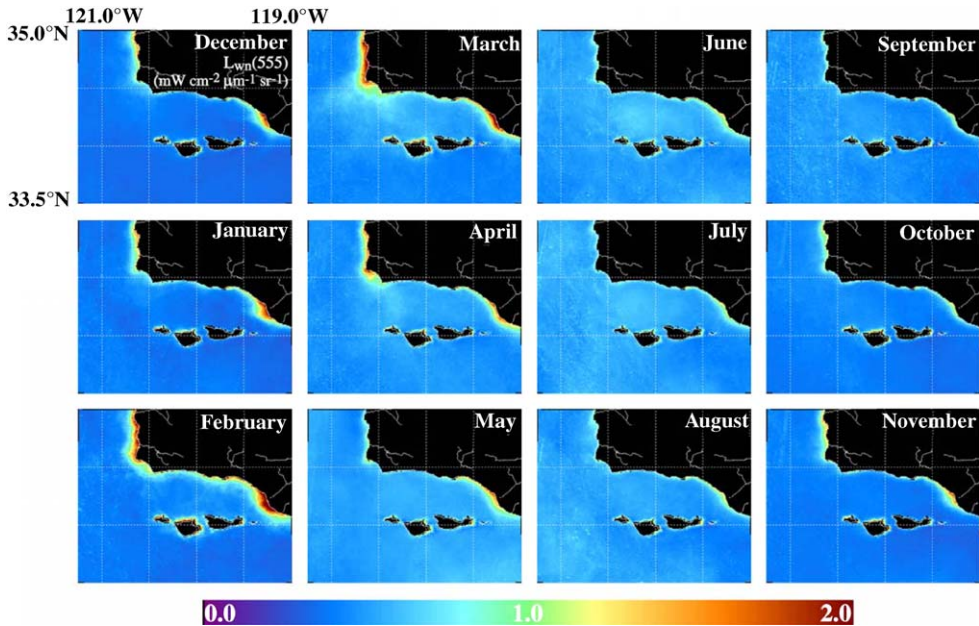


Fig. 6.  $L_{WN}(555)$  monthly mean annual cycle computed from all available images. Images above are composites of all data from each month. The monthly mean annual cycle is computed from October 1997 to June 2001.

found within the SBC. Chl concentrations decrease in the eastern portion of the channel first, then in the west as summer progresses and poleward flows bring warmer, nutrient-poor waters from the east. The lowest monthly mean Chl values range from 0.5 to 1.0 mg m<sup>-3</sup> and are observed in September corresponding to the warmest SSTs. Nearshore Chl patterns are not always related to SST, which is most obvious in the winter (December–February) when upwelling is at a minimum while nearshore Chl values are high. The resulting pattern is consistent with blooms induced by terrestrial runoff from storms.

Elevated monthly mean values of  $L_{wN}(555)$  ( $>1.0 \text{ mW cm}^{-2} \mu\text{m}^{-1} \text{ sr}^{-1}$ ) are found near the mouths of the Santa Clara, Santa Ynez and Santa Maria rivers from winter to spring, indicating the presence of sediment plumes (Fig. 6). The greatest extent of these plumes is found in February when the largest storms of the year occur. Also, subtle variations in  $L_{wN}(555)$  are observed offshore (Fig. 6) where offshore  $L_{wN}(555)$  values increase by about a factor of two from fall to spring. This is similar to the seasonal changes in Chl and likely represents changes in particulate backscatter by phytoplankton.

### 3.3. Temporal variability and covariability of the Santa Barbara Channel

Minimum SSTs for the SBC region consistently occur in the spring due to the onset of upwelling (Fig. 7A). The warmest SSTs are found in late summer and early fall due to a combination of seasonal warming and the poleward advection of Southern California Bight waters. The amplitude of the SST seasonal cycle varies dramatically and illustrates the impact of the 1997–1998 El Niño and ensuing La Niña conditions (Fig. 7A). The maximum SBC mean SST (19.2 °C) occurred near the start of the time-series during the local peak in El Niño conditions (Dever and Winant, 2002), while the cool summer and fall of 1999 occurred during La Niña conditions. The lowest mean SST (12.0 °C) is observed in April 2001.

Regional mean Chl concentrations follow a rough inverse relationship with SST (Fig. 7B). Chl concentrations are highest during spring and

show considerable interannual variations in the magnitude and duration of these peak events. The highest regional mean Chl values are 3.7 and 4.1 mg m<sup>-3</sup> and are observed for the months of May 2000 and April 2001, respectively. Despite record highs for upwelling indices in the spring of 1999 for this region (Schwing et al., 2000), Chl values remain less than 2 mg m<sup>-3</sup> (Fig. 7B). The lowest Chl values observed (0.5 mg m<sup>-3</sup>) are found during the El Niño peak of October and November 1997. After the fall of 1998, mean Chl values are rarely less than 1 mg m<sup>-3</sup>.

Temporal variations in the SBC mean  $L_{wN}(555)$  appear to be the superposition of two distinct signals (Fig. 7C). The first is a low-amplitude seasonal cycle oscillating between 0.4 and 0.6 mW cm<sup>-2</sup> μm<sup>-1</sup> sr<sup>-1</sup> with a maximum in the spring–summer with little significant interannual variation. This signal corresponds to periods when SBC Chl levels are greater than ~1.3 mg m<sup>-3</sup>, suggesting it is caused by phytoplankton backscatter. The second signal corresponds to large and episodic increases in late winter due to runoff events. The highest SBC mean  $L_{wN}(555)$  value appears coincident with the large discharge events that occurred during the 1997/1998 El Niño.

Time-series of monthly mean wind stress at the west channel buoy and daily discharge from the Santa Clara River are presented to illustrate the roles of local forcing on SBC mean properties (Fig. 7D). Wind stress along the major principal axis (toward ESE, 122° clockwise from north) is at its maximum during summer (monthly means range from 0.13 to 0.24 N m<sup>-2</sup>) while minimum wind stresses occur during winter ( $<0.1 \text{ N m}^{-2}$ ). Large interannual variations in monthly mean wind stress are observed with periods of weak winds in the summer of 1998 and strong winds in the spring of 1999 (Fig. 7D).

Discharge records from the Santa Clara River are highly episodic (Fig. 7E). Maximum flow occurs typically in late winter and early spring while baseflow is often negligible. The 1997/1998 El Niño was an exceptionally wet year. Large discharge events are observed and baseflow remained high for the entire hydrologic year (defined October 1–September 30). Discharge

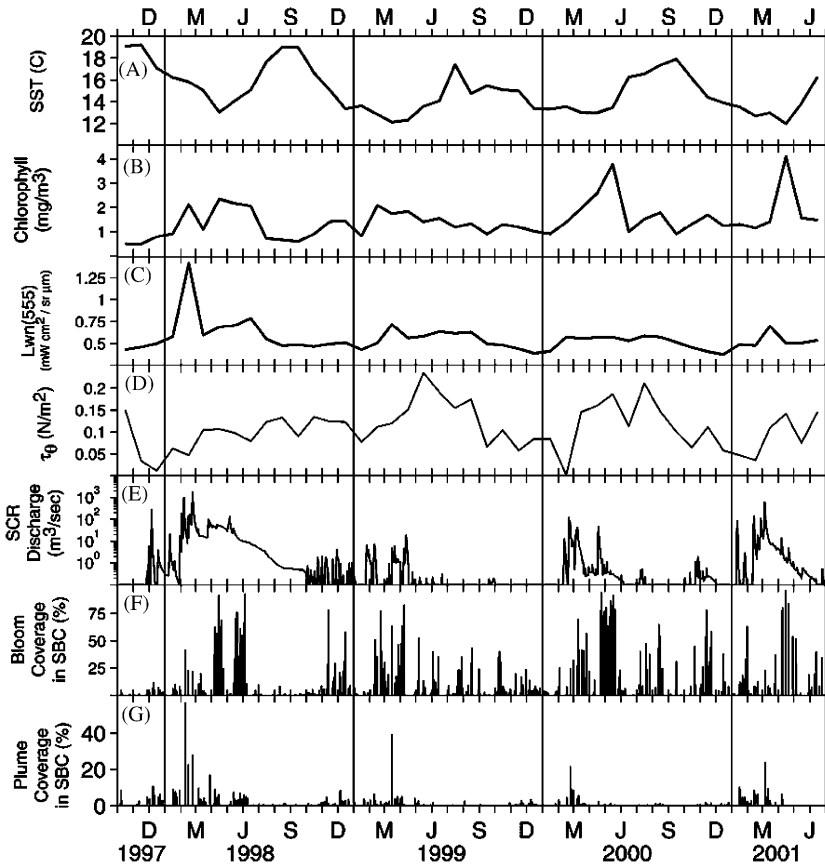


Fig. 7. SBC regional mean time-series of (A) SST, (B) Chl and (C)  $L_{wN}(555)$  averaged on a monthly basis. Only scenes with a minimum of 70% coverage (88% coverage for SST) are used in computing spatial averages over the SBC. Local forcing by (D) wind stress at the west channel buoy along the principal axis (aligned  $122^\circ$  clockwise from north) and (E) daily discharge from the Santa Clara River as measured by the USGS. Percent of the SBC covered by (F) blooms and (G) plumes. Percent coverage calculations are only computed for images with greater than 80% data coverage over the SBC for Chl and greater than 70% data coverage over the SBC for  $L_{wN}(555)$ .

was small in 1999 and only a bit larger in the following years (Fig. 7E). Except for 1999, between 65% and 90% of total annual discharge occurs over a few events during February and March of each year.

Significant correlations (0.87, 99% significant level; Table 2) are found between SBC mean values of  $L_{wN}(555)$  and monthly mean discharge records for the Santa Clara River, indicating that sediment plumes dominate the  $L_{wN}(555)$  signal. This correlation is not driven by the one big event in February 1998, as the correlation remains significant (0.50, 99% significant level) after removing observations for that month. Monthly regional

mean values of SST and Chl are inversely correlated, but this linear relationship accounts for only 33% of the variance (Table 2). Insignificant correlations (at the 99% level) are observed between wind stress and any regional mean property (Table 2). The fact that the maximum mean Chl and the minimum mean SST occurs in spring works against a correlation with wind stress, as maximum mean winds are found in the summer when retrievals of Chl (SST) are declining (rising). Hence, spatial patterns on scales smaller than the SBC, such as those induced by advection and the development of gradients, must be considered.

The importance of remote forcing, such as the occurrence of El Niño and La Niña events, can be assessed by examining annual means computed over the hydrologic years where we have complete satellite observations (Table 3). The negative mean SOI value for 1997–1998 indicates El Niño conditions, while positive mean SOI values in subsequent years indicate La Niña conditions. Differences between El Niño and La Niña conditions are evident in annual mean values of local forcing and SBC average values of SST and  $L_{wN}(555)$  (Table 3). Comparing El Niño–La Niña conditions, annual mean SST dropped by  $\sim 2^\circ\text{C}$  while values of upwelling favorable wind stress increase by 40%. Mean Chl values are only slightly higher in 1998–1999 compared with El Niño conditions (Table 3). Both  $L_{wN}(555)$  and the annual Santa Clara River discharge are considerably higher for 1997–1998 compared with the other years.

Interannual variations for most remotely sensed variables over the SBC are consistent with forcing by the El Niño–La Niña cycle using the SOI as an index (Table 2). Correlations are performed

between the SOI and monthly anomalies of the regional property or forcing factor. As expected, monthly anomalies of SBC mean SST are correlated with SOI estimates ( $r = -0.60$ ; significant at 99% c.i.). Insignificant correlation is found between the SOI and the anomalous wind stress (Table 2). Although there is no robust statistical link, weaker upwelling favorable winds are observed during the El Niño, which may have contributed to warm SST anomalies in late summer (Figs. 7A and D). For the El Niño year, annual mean Chl concentrations are lower than for other years, but these differences are not very dramatic (Table 3). Anomalies in both Santa Clara River discharge and  $L_{wN}(555)$  are well correlated with the SOI.

The lack of simple correlations between SBC regional mean properties and wind suggests that non-local processes are likely participants in the observed interannual variations. Anomalous poleward flows were observed through the SBC in spring 1999 relative to the long-term mean as well as years 1998 and 2000 (Lynn et al., 1998; Hayward et al., 1999; Bograd et al., 2000; Dever

Table 2  
Correlation coefficients<sup>a</sup> for satellite data and local forcing

	SOI <sup>a</sup>	$\tau_x$	$\tau_y$	$\tau_\theta$	SCR	$L_{wN}(555)$	Chl
SST	<b>-0.60</b>	-0.03	0.10	-0.05	-0.04	-0.06	<b>-0.58</b>
Chl	0.14	0.32	-0.31	0.32	0.18	0.31	
$L_{wN}(555)$	<b>-0.41</b>	0.02	0.00	0.02	<b>0.87</b>		
SCR	<b>-0.46</b>	-0.24	0.20	-0.24			
$\tau_\theta$	0.16	<b>0.99</b>	<b>-0.96</b>				
$\tau_y$	-0.05	<b>-0.91</b>					
$\tau_x$	0.21						

Bold values are significant at the 99% confidence level (0.346,  $n = 45$ ) and SCR represents discharge from the Santa Clara River.

<sup>a</sup>Correlations with the SOI are between the SOI and monthly anomalies of the variable.

Table 3  
Hydrologic year means for satellite data, local forcing and the SOI

Hydrologic year	SBC SST (°C)	SBC Chl ( $\text{mg m}^{-3}$ )	SBC $L_{wN}(555)$ ( $\text{mW sr}^{-1} \mu\text{m}^{-1} \text{cm}^{-2}$ )	$\tau_x$ ( $\text{N m}^{-2}$ )	$\tau_y$ ( $\text{N m}^{-2}$ )	$\tau_\theta$ ( $\text{N m}^{-2}$ )	SOI	Cumulative SCR ( $10^7 \text{m}^3$ )
1997–1998	16.7	1.2	0.64	0.07	-0.05	0.09	-0.97	83.95
1998–1999	14.3	1.4	0.55	0.12	-0.08	0.14	0.76	1.44
1999–2000	14.8	1.6	0.52	0.10	-0.06	0.12	0.72	6.21

and Winant, 2002). This suggests that these poleward flows advected nutrient-poor, Southern California Bight waters through the channel during the 1999 La Niña, which would explain the relatively small spring bloom found then. The largest spring blooms occur in 2000 and 2001 (Fig. 7B), suggesting that El Niño and La Niña reduce SBC mean Chl by disturbing the flows of nutrient rich upwelled waters. The large La Niña event of 1999 induced strong poleward flows through the channel, presumably reducing the available nutrient supply, while, during the strong El Niño of 1998, the depth of the nitracline is simply too deep to allow the effective upwelling of nutrient rich waters (data not shown). Hence, the highest regional Chl concentrations occurred under intermediate El Niño conditions.

#### 3.4. Indices for sediment plume and phytoplankton bloom events

Indices for the occurrence of a “plume” and/or “bloom” are developed to describe the extent and duration of phytoplankton blooms and sediment plumes in the SBC. Simple threshold indices are used where the determination of the threshold level is subjective in nature. Blooms will be denoted if Chl exceeds  $2 \text{ mg m}^{-3}$ , while pixels are classified as a plume if  $L_{wN}(555)$  exceeds  $1.3 \text{ mW cm}^{-2} \mu\text{m}^{-1} \text{ sr}^{-1}$ . Guidance for these threshold levels comes from analyzing the available field and satellite data (Toole and Siegel, 2001; Otero, 2002). These indices independently identify conditions suggesting the presence of a phytoplankton bloom and/or a sediment plume and are not meant to distinguish between these two conditions.

Frequencies of occurrence distributions of bloom indices show blooms occur most frequently (60–80% of the time) around the Santa Clara River mouth and north of Point Arguello (Fig. 8A). Blooms also occur frequently, ~25% of images, in the western portion of the SBC, while they are found less frequently in the east channel. For the Channel Islands, frequent plume indices are only found for Santa Rosa Island. Extensive blooms covering more than 50% of the channel occur during the spring and last about 1 month

(Fig. 7F). These blooms occur concurrently with an increase in wind stress and a decline in mean SST. Smaller blooms also are observed throughout the year (Fig. 7F).

Good correspondence is observed between SBC plume coverage and the Santa Clara River discharge on episodic and seasonal timescales (Figs. 7E and G). Events with large surface plume extent occur during single days in February and March coincident with large runoff events. The largest plume event observed covered 58% of the SBC during February 1998. Observations of surface plumes for 2000 and 2001 are similar in size, covering at most 20% of the channel. Unusual events also are observed. On March 16, 1999, the plume index suggests that plumes are covering ~40% of the channel although runoff preceding this is small (Figs. 7E and G). Analysis of phytoplankton pigment distributions indicates that this “plume” event is likely to be a coccolithophorid bloom (see Otero, 2002 for details and figures). Although this is a rare occurrence, it does point to limitations of simple classification indices. Ignoring the March 1999 event, the spatial extent of plume coverage over the SBC shows the expected relationship where larger discharge events correspond to larger sediment plume coverage.

#### 3.5. Modal analyses of time/space variability

In order to distinguish between the spatial effects of upwelling and terrestrial runoff, monthly composites of SST, Chl and  $L_{wN}(555)$  are decomposed using EOF analysis (Lagerloef and Bernstein, 1988; Emery and Thomson, 2001). An EOF analysis organizes a time/space series into a set of orthogonal functions that compactly describe the covariability of the data set. This will be provided in the form of a ranked set of spatial maps whose amplitude varies in time about a mean state. The ranking provides a measure of the fraction of total variance explained by each EOF mode. Typically, the lowest modes explain much of the variance and these spatial/temporal patterns will be the easiest to interpret. The few gaps in the data sets are filled by averaging (see Otero, 2002 for details).

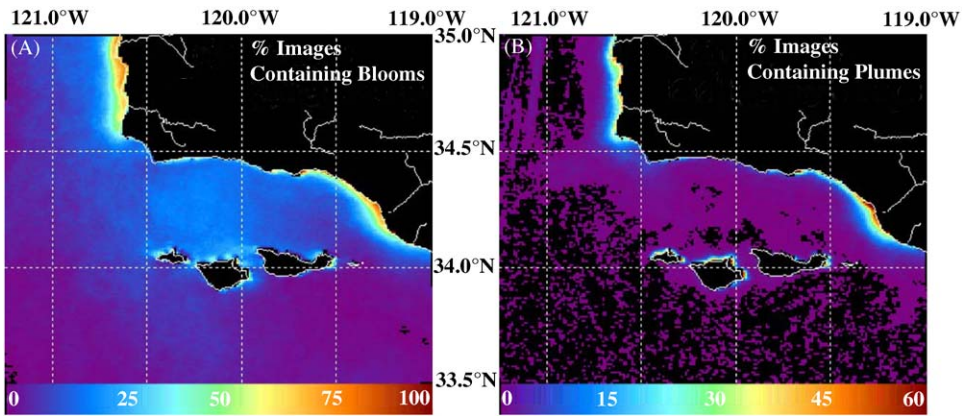


Fig. 8. Maps showing the frequency of (A) blooms and (B) plumes using the indices defined by Otero (2002). Pixels exceeding  $2 \text{ mg m}^{-3}$  Chl are denoted a bloom while pixels are classified as a plume if  $L_{wN}(555)$  exceeds  $1.3 \text{ mW cm}^{-2} \mu\text{m}^{-1} \text{ sr}^{-1}$ . Frequency is expressed in terms of the percentage of images where values exceed the plume or bloom threshold.

The first mode of the SST field (Fig. 9A) clearly resembles the mean state, while its amplitude function corresponds to the seasonal cycle (Fig. 10A); maximum SST in late summer–early fall and minimum temperatures during upwelling in spring. This mode dominates as it represents 91.3% of the temporal variance. As expected, the amplitude function is highly correlated with the SBC mean SST and is significantly anti-correlated with the SBC mean Chl (Table 4). However, it is not related to wind in a simple way.

The second SST EOF mode contains 4.7% of the variance, and its spatial pattern is roughly similar to the first SST mode except that the east–west gradient is accentuated showing the characteristics of an “upwelling-like” pattern (Fig. 9B). Negative values are found off of Point Arguello, while strongly positive values are found east of the SBC. Its amplitude function leads the first mode’s amplitude function by 1–3 months (lagged correlation with the second mode leading is only significant at 2 months at the 99% confidence level, Fig. 10B). This mode is well correlated with wind stress (Table 4) and demonstrates a relationship between wind-driven upwelling and the intensification of the along-channel SST gradient (Lagerloef and Bernstein, 1988).

The third SST mode contains 1.6% of the total variance. It appears related to the advection of

upwelled waters into the SBC as the coolest waters are found along the continental shelf north of Point Conception and in the western channel, while the warmest waters are found far offshore (Fig. 9C). Its amplitude function is highly variable (Fig. 10C) and is not significantly correlated with any of the forcing factors in Table 4.

The first Chl EOF mode contains 42.5% of the variance and is positive everywhere with its largest signals occurring along the coast, north of Point Arguello, and in the western SBC (Fig. 11A). A similar spatial pattern is observed in the frequency of blooms (Fig. 8A) with the important exception that high values are not found near the Santa Clara River. The amplitude function shows seasonal oscillations between spring–summer and fall–winter (Fig. 12A) and is highly correlated with the SBC mean Chl. It also is significantly correlated with SBC mean SST and wind stress, suggesting a role for upwelling (Table 4). With the exception of low winds observed for 1998, annual maxima in wind stress correspond well with positive periods in the amplitude function.

The second Chl EOF mode (12.4% of the variance) shows an inverse relationship between Chl anomalies throughout the SBC, particularly in the vicinity of the Santa Clara River, and those along the coast north of Point Arguello (Fig. 11B). Its amplitude function is positive from fall to early

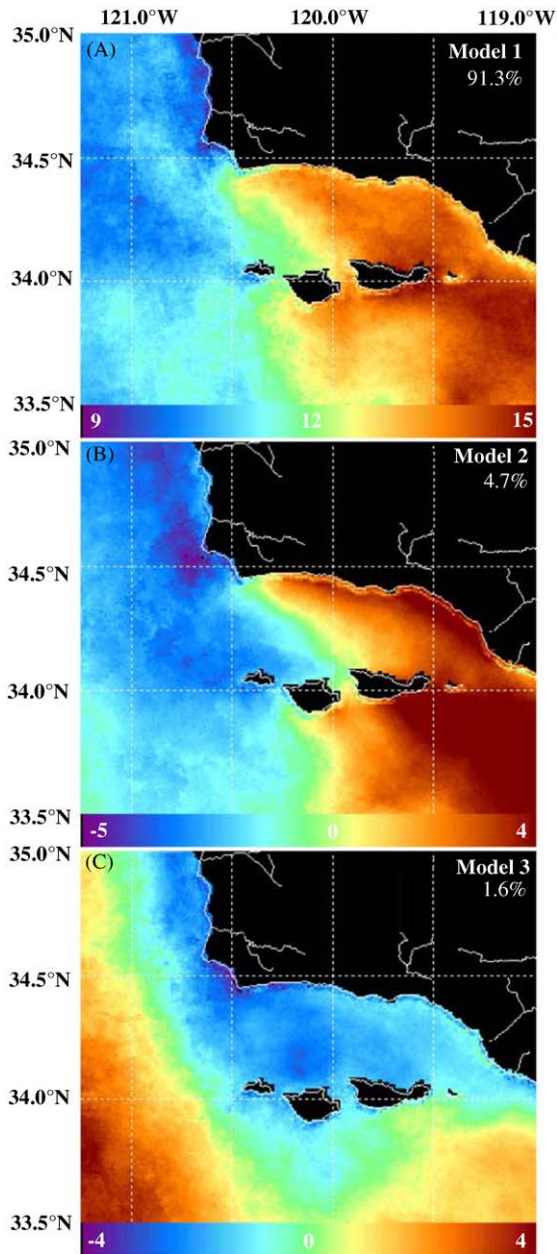


Fig. 9. (A) First, (B) second and (C) third mode from temporal EOF analysis of SST. Positive amplitudes in Fig. 10 correspond to positive and negative anomalies as shown here while negative amplitudes reverse the signs of the anomalies.

spring and negative from late spring to summer (Fig. 12B). This indicates that Chl values are higher from fall to early spring near the Santa

Clara River relative to those on the shelf north of Point Arguello. Weak correlations are observed with the zonal-component of wind stress, SST and Chl itself suggest a relationship with upwelling (Table 4). Stronger correlations with wind are not observed as negative phase of the modal amplitudes lag increases in upwelling favorable winds by 1–2 months. However, from late spring to summer, negative modal amplitudes and upwelling favorable winds do correspond. This is consistent with upwelling processes and elevated Chl values north of Point Arguello through the summer as seen in the climatology for Chl (Fig. 5). A weak correlation also is seen with Santa Clara River discharge (Table 4), although this correlation becomes insignificant when data from February 1998 are removed. However, the amplitude time-series corresponds with seasonal increases in Santa Clara River discharge from winter to early spring (Fig. 12B), suggesting that positive amplitudes may represent long-term seasonal flow instead of episodic events. Overall, the second Chl EOF mode represents forcing by two seasonal signals: (1) upwelling in late spring and summer to the north of Point Arguello and (2) seasonal discharges from winter to early spring near the Santa Clara River. In all, this mode captures the transition from winter to summer conditions in Chl.

The largest anomalies in the third Chl mode (6.5% of total variance) are found along the entire mainland coast of the SBC (Fig. 11C). The amplitude function is episodic, with a positive signal during February 1998 when extreme flooding associated with El Niño took place and a smaller negative event for April 2001 (Fig. 12C). Significant correlations are observed with the SBC mean  $L_{wN}(555)$ , Santa Clara River discharge, and the SOI (Table 4), but are insignificant (except  $L_{wN}(555)$ ) when February 1998 is removed from the correlation. All told, this mode is associated with episodic runoff.

The first  $L_{wN}(555)$  mode contains 51.4% of the temporal variance and shows positive anomalies along the mainland coast with the largest anomalies near major river mouths (Fig. 13A). Santa Rosa Island also shows large positive anomalies around it, larger than those found for the other

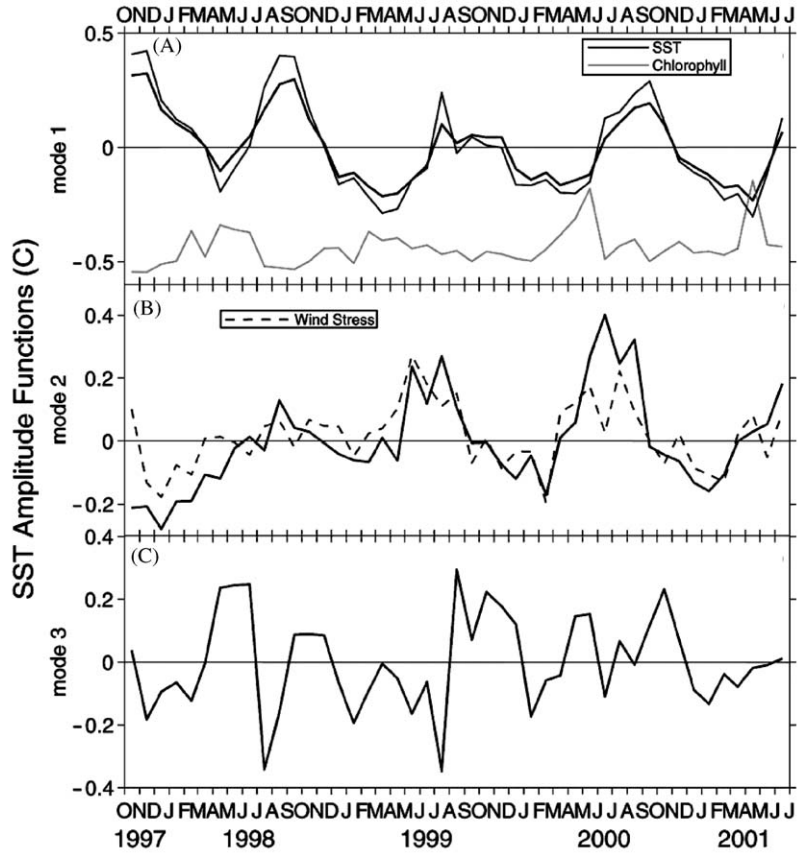


Fig. 10. (A) First, (B) second and (C) third amplitude function from temporal EOF analysis of SST. All properties plotted with amplitude functions are scaled to each amplitude’s range. SST and Chl are SBC regional mean values.

Table 4  
Correlation coefficients<sup>a</sup> between EOF amplitude functions and satellite data, local forcing and the SOI

Temporal mode	% variance	SBC SST	SBC Chl	SBC $L_{wN}(555)$	$\tau_x$	$\tau_y$	$\tau_\theta$	SCR	SOI
SST 1	91.3	<b>0.99</b>	<b>-0.56</b>	-0.05	-0.08	0.14	-0.10	-0.03	-0.29
SST 2	4.7	0.08	0.24	0.00	<b>0.75</b>	<b>-0.53</b>	0.70	-0.27	0.17
SST 3	1.6	-0.13	0.30	0.00	0.05	-0.08	0.06	-0.06	0.03
Chl 1	42.5	<b>-0.41</b>	0.90	0.23	<b>0.52</b>	<b>-0.44</b>	0.51	0.05	0.01
Chl 2	12.4	<b>-0.49</b>	0.41	0.28	<b>-0.35</b>	0.17	-0.30	<b>0.39</b>	-0.06
Chl 3	6.5	0.11	0.00	<b>0.73</b>	-0.13	0.13	-0.14	<b>0.73</b>	<b>-0.39</b>
$L_{wN}(555)$ 1	51.4	-0.10	0.21	<b>0.92</b>	-0.19	0.15	-0.18	<b>0.95</b>	<b>-0.44</b>
$L_{wN}(555)$ 2	18.0	0.01	0.33	0.34	<b>0.70</b>	<b>-0.52</b>	0.66	-0.01	0.12
$L_{wN}(555)$ 3	5.2	<b>0.37</b>	-0.13	0.12	-0.16	0.23	-0.18	0.14	0.00

<sup>a</sup>Bold values are significant at the 99% confidence level (0.346,  $n = 45$ ) and SCR represents discharge from the Santa Clara River.

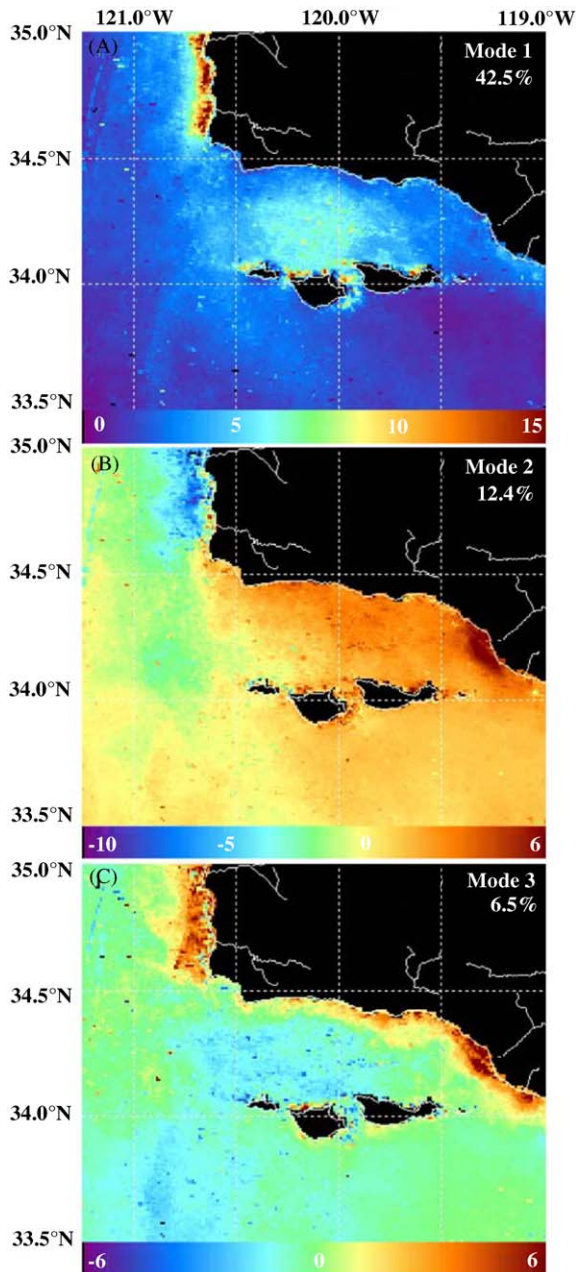


Fig. 11. (A) First, (B) second and (C) third mode from temporal EOF analysis of Chl. Positive amplitudes in Fig. 12 correspond to positive and negative anomalies as shown here while negative amplitudes reverse the signs of the anomalies.

Northern Channel Islands (e.g., Mertes et al., 1998). The first  $L_{wN}(555)$  amplitude function peaks in February or March of each year

(Fig. 14A) and is very well correlated with discharge from the Santa Clara River and SBC mean  $L_{wN}(555)$  (Table 4). The amplitude function remains highly correlated with discharge ( $r = 0.75$  vs. 0.95) when data from February 1998 are removed from consideration. This mode clearly represents the effects of surface sediments on  $L_{wN}(555)$ .

The second  $L_{wN}(555)$  mode, containing 18.0% of the variance, has a structure with positive anomalies offshore and negative anomalies near major river mouths (Fig. 13B). Similar to the second Chl mode, the amplitude function changes sign seasonally, being positive offshore from April to September then positive nearshore for the remainder of the year (Fig. 14B). Significant correlations are observed with wind stress indices (Table 4), and the amplitude function corresponds well with increases in upwelling favorable winds (Fig. 14B). This suggests that the positive anomalies offshore during spring and summer correspond to backscatter from phytoplankton blooms. Negative amplitudes are found during fall and winter, corresponding to positive anomalies that resemble the plume index pattern (Fig. 8B). This suggests that during fall and winter, this mode represents seasonal river discharge. Overall, this mode, like the second Chl EOF mode, represents a transition from winter to summer conditions.

The third  $L_{wN}(555)$  mode (5.2% of the variance) has strong positive anomalies along the coast near Point Arguello and northward and weak negative anomalies in the SBC and offshore (Fig. 13C). The amplitude function shows positive values in March of each year (Fig. 14C). Although it does not correlate well with any of the forcings discussed (Table 4), the time course of the amplitude appears driven by late-event runoff.

The spatial effects of upwelling and runoff are clearly captured in the two first EOF modes for Chl and  $L_{wN}(555)$ , respectively. The first Chl mode reveals the characteristic upwelling pattern of elevated Chl north of Point Arguello and in the western channel from spring to summer. Alternatively, the first  $L_{wN}(555)$  mode captures characteristic surface sediment plume patterns following episodic runoff events in February and

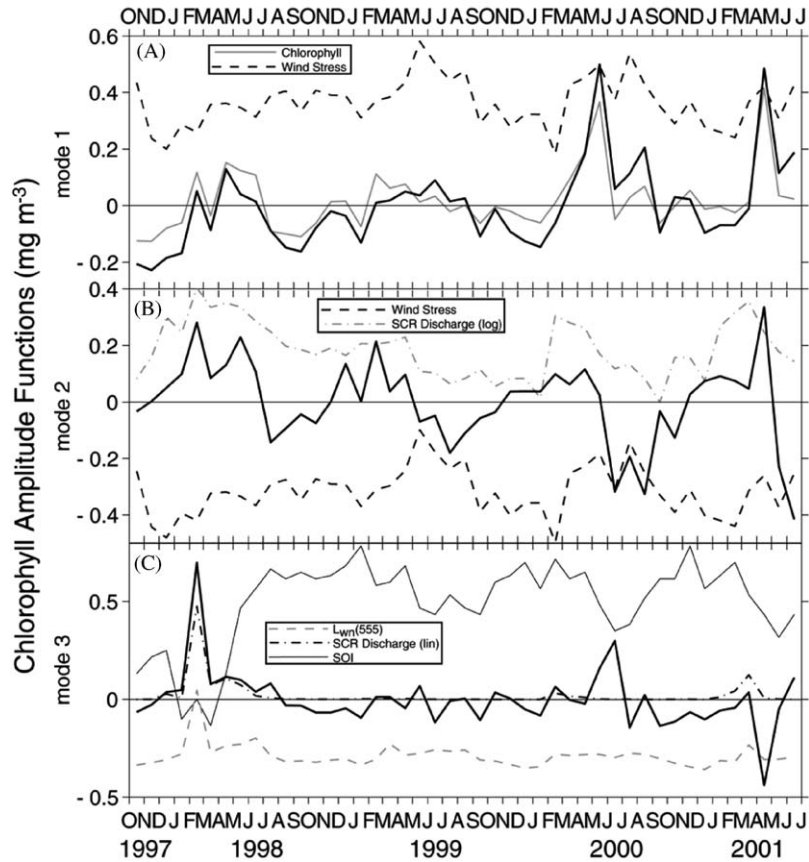


Fig. 12. (A) First, (B) second and (C) third amplitude function from temporal EOF analysis of Chl. All properties plotted with amplitude functions are scaled to each amplitude's range. Chl and  $L_{wN}(555)$  correspond to SBC regional mean values. SCR is Santa Clara River discharge shown in log (log) and linear (lin) scales to emphasize seasonal and episodic features, respectively.

March. Both of their second modes appear to represent a transition from runoff-dominated processes in winter to upwelling- and bloom-dominated processes in summer. In the Chl mode, this means elevated values near the Santa Clara River in association with runoff during winter and a transition to elevated values north of Point Arguello in association with upwelling in summer. For  $L_{wN}(555)$ , positive anomalies are observed near the Santa Clara River and north of Point Arguello in association with runoff during winter which transition to positive anomalies offshore, away from sediment-dominated regions, during summer in association with increased Chl concentrations.

#### 4. Summary and conclusions

Using validated remote sensing and supporting environmental data sets, we have shown that coastal upwelling and terrestrial runoff are two major processes dominating variations in water turbidity and phytoplankton biomass for the SBC. On seasonal timescales, the largest blooms are associated with cool upwelled waters in spring while elevated nearshore Chl and  $L_{wN}(555)$  values are related to sediment plumes from terrestrial runoff in late winter. Significant correlations between local forcing and monthly SBC regional mean values were found only between  $L_{wN}(555)$  and the Santa Clara River discharge. SST and Chl

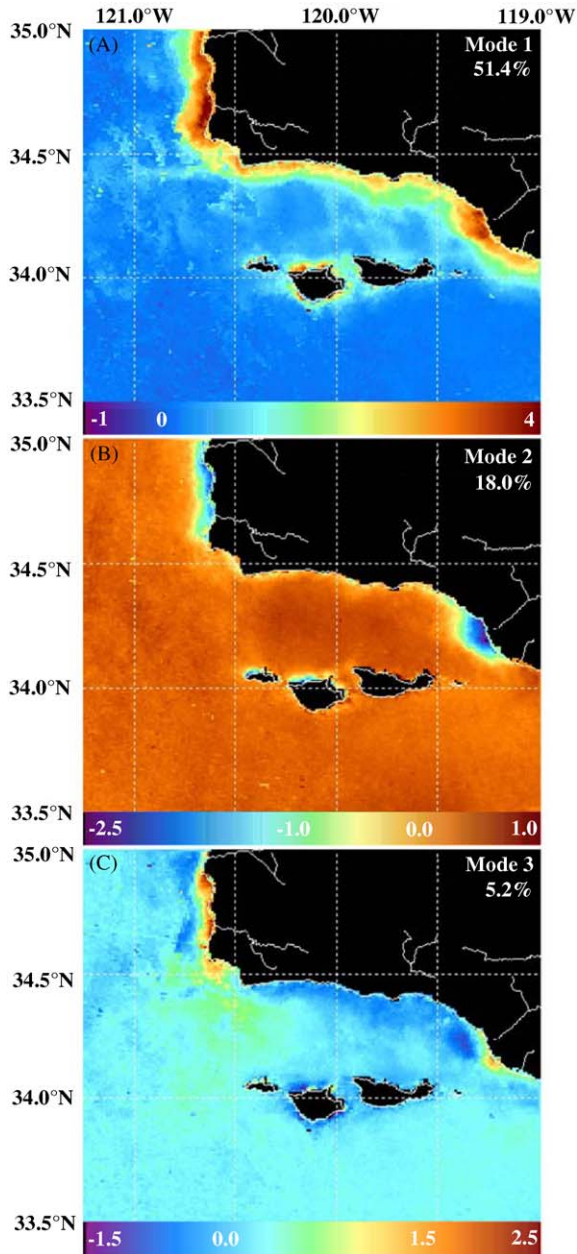


Fig. 13. (A) First, (B) second and (C) third mode from temporal EOF analysis of  $L_{wN}(555)$ . Positive amplitudes in Fig. 14 correspond to positive and negative anomalies as shown here, while negative amplitudes reverse the signs of the anomaly.

variations are driven by a coupling of advection and upwelling processes, and are not simply correlated to a single local forcing index.

Observed interannual variations are consistent with forcing by El Niño/La Niña cycles. During the 1997/1998 El Niño, SST values were high, upwelling favorable wind stress weak, SBC mean Chl was fairly low and extreme terrestrial discharges produced high  $L_{wN}(555)$  throughout the SBC. Significant correlations are found between SOI and SST and for SOI and  $L_{wN}(555)$  due to the extreme floods of February 1998. However, SBC mean Chl changes do not follow this simple pattern, as the highest, springtime Chl values are found for neither El Niño nor La Niña conditions. It is suggested that the advection of nutrient-depleted waters from the east is driving these interannual differences in Chl values.

A simple classification analysis shows that plumes are confined to the mainland continental shelf regions, while blooms extend offshore and are observed more frequently in the western portion of the SBC. Large surface plumes, covering >20% of the channel, are observed about once per year, and during the 1997/1998 El Niño floods plumes covered nearly 60% of the channel. Large blooms occur most frequently during the spring and can cover up to 95% of the SBC.

The effects of upwelling and runoff processes are temporally and spatially resolved from one another using EOF analyses. The first Chl mode, containing 43% of the temporal variance, is associated with upwelling and shows a spatial pattern with elevated Chl values in the western SBC and nearshore north of Point Arguello. Episodic discharge events dominate the first  $L_{wN}(555)$  mode containing 51% of the variance. In this mode, anomalies are largest nearshore and positive throughout the channel while the amplitude function is well correlated with discharge from the Santa Clara River. The transition from runoff-dominated processes in winter to upwelling- and bloom-dominated processes in summer is represented in the second EOF modes of both Chl and  $L_{wN}(555)$  containing 12% and 18% of the temporal variance, respectively. In all, local processes appear to have the dominant control of sediment plumes and phytoplankton blooms within the SBC, though it remains difficult to ascribe their regulation on a single set of forcing indices.

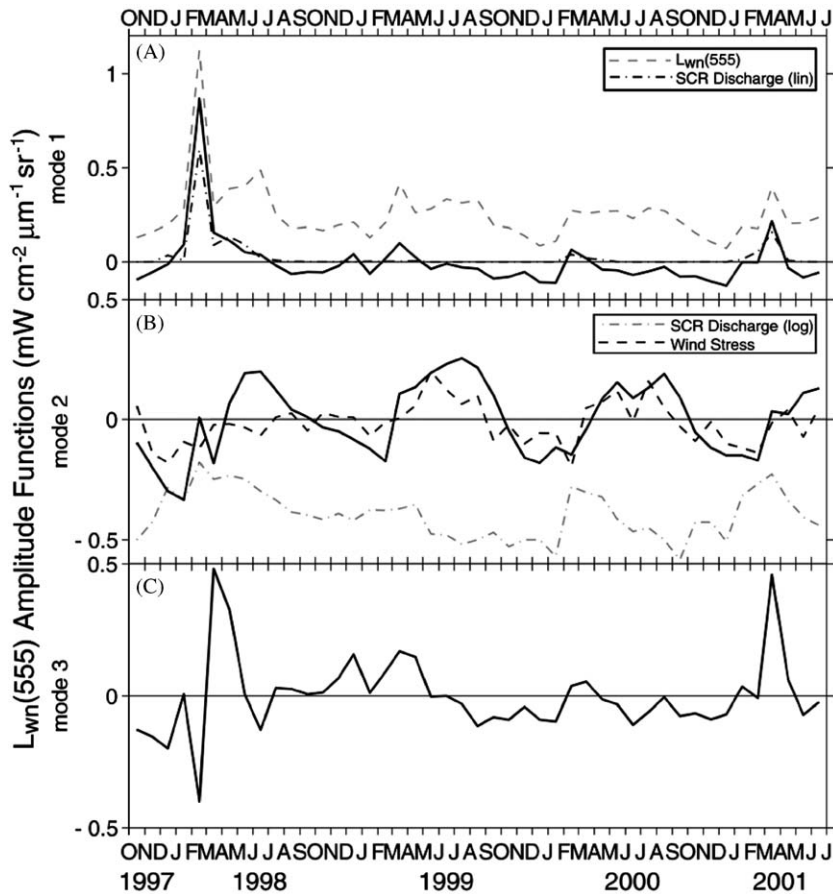


Fig. 14. (A) First, (B) second and (C) third amplitude function from temporal EOF analysis of  $L_{wN}(555)$ . All properties plotted with amplitude functions are scaled to each amplitude's range. SCR is Santa Clara River discharge shown in log (log) and linear (lin) scales to emphasize seasonal and episodic features, respectively.  $L_{wN}(555)$  corresponds to SBC regional mean values.

### Acknowledgements

Support for this work comes from the NASA, NOAA, Channel Islands National Marine Sanctuary, and NSF as part of the Plumes and Blooms and Santa Barbara Coastal LTER research programs. SeaWiFS images are provided by the Orbital Sciences Corporation and the NASA Goddard Space Flight Center. The authors would like to thank the Plumes and Blooms team for their hard work and dedication. Finally, we would thank the following people for valuable discussions and contributions pertaining to this work: Erik Fields, Manuela Lorenzi-Kayser, Libe Washburn, Mark Brzezinski, Carter Ohlmann, DeDe

Toole, Toby Westberry, Olga Polyakov, Jon Warrick, Leal Mertes, Ed Dever, Stephane Maritorena, Nathalie Gillocheau, David Menzies, Sarah Fangman, Deborah Fernamburg, Michael Neumann, Jens Sorenson and Raymond Smith.

### References

- Atkinson, L.P., Brink, K.H., Davis, R.E., Jones, B.H., Paluszkiwicz, T., Stuart, D.W., 1986. Mesoscale hydrographic variability in the vicinity of Points Conception and Arguello during April–May 1983: the OPUS 1983 experiment. *Journal of Geophysical Research* 91, 12899–12918.
- Bograd, S.J., DiGiacomo, P.M., Durazo, R., Hayward, T.L., Hyrenbach, K.D., Lynn, R.J., Mantyla, A.W., Schwing,

- F.B., Sydeman, W.J., Baumgartner, T., Lavaniegos, B., Moore, C.S., 2000. The state of the California Current: forward to a new regime? *California Cooperative Oceanic Fisheries Investigations Reports* 41, 26–52.
- Brink, K.H., Stuart, D.W., Van Leer, J.C., 1984. Observations of the coastal upwelling region near 34°30'N off California: spring 1981. *Journal of Physical Oceanography* 14, 378–391.
- Campbell, J.W., Blaisdell, J.M., Darzi, M., 1995. Level-3 SeaWiFS data products: spatial and temporal binning algorithms. In: Hooker, S.B., Firestone, E.R., Acker, J.G. (Eds.), *SeaWiFS Pre-launch Technical Report Series*, Vol. 32. NASA TM 104566. Goddard Space Flight Center, Greenbelt, MD.
- Dever, E.P., Winant, C.D., 2002. The evolution and depth structure of shelf and slope temperatures and velocities during the 1997–1998 El Niño near Pt. Conception, California. *Progress in Oceanography* 54, 77–103.
- Dorman, D.E., Winant, C.D., 2000. The structure and variability of the marine atmosphere around the Santa Barbara Channel. *Monthly Weather Review* 128, 261–282.
- Emery, W.J., Thomson, R.E., 2001. *Data Analysis Methods in Physical Oceanography*, 2nd Edition. Elsevier, Amsterdam, pp. 305–370.
- Eppley, R.W., Renger, E.H., Harrison, W.G., 1979. Nitrate and phytoplankton production in southern California coastal waters. *Limnology and Oceanography* 24, 483–494.
- Harms, S., Winant, C.D., 1998. Characteristic patterns of the circulation in the Santa Barbara Channel. *Journal of Geophysical Research* 103, 3041–3065.
- Haston, L., Michaelsen, J., 1994. Long-term central coastal California precipitation variability and relationships to El Niño-Southern Oscillation. *Journal of Climate* 7, 1373–1387.
- Hayward, T.L., Venrick, E.L., 1998. Nearsurface pattern in the California Current: coupling between physical and biological structure. *Deep-Sea Research II* 45, 1617–1638.
- Hayward, T.L., Baumgartner, R.R., Checkley, D.M., Durazo, R., Gaxiola-Castro, G., Hyrenbach, K.D., Mantyla, A.W., Mullin, M.M., Murphree, T., Schwing, F.B., Smith, P.E., Tegner, M.J., 1999. The state of the California Current in 1998–1999: transition to cool-water conditions. *California Cooperative Oceanic Fisheries Investigations Reports* 40, 29–62.
- Hickey, B.M., 1979. The California Current System—hypotheses and facts. *Progress in Oceanography* 8, 191–279.
- Hickey, B.M., Dobbins, E.L., Allen, S.E., 2003. Local and remote forcing of currents and temperature in the central Southern California Bight. *Journal of Geophysical Research* 108, 3081.
- IOCCG, 2000. Remote sensing of ocean colour in coastal, and other optically complex waters. In: Sathyendranath, S. (Ed.), *Reports of the International Ocean-Colour Coordinating Group*, No. 3. IOCCG, Dartmouth, Canada.
- Inman, D.L., Jenkins, S.A., 1999. Climate change and the episodicity of sediment flux of small California rivers. *Journal of Geology* 107, 251–270.
- Jones, B.H., Atkinson, L.P., Blasco, D., Brink, K.H., Smith, S.L., 1988. The asymmetric distribution of chlorophyll associated with a coastal upwelling center. *Continental Shelf Research* 8, 1155–1170.
- Kahru, M., Mitchell, G.B., 1999. Empirical chlorophyll algorithm and preliminary SeaWiFS validation for the California Current. *International Journal of Remote Sensing* 20, 3423–3429.
- Lagerloef, G.S., Bernstein, R.L., 1988. Empirical orthogonal function analysis of advanced very high resolution radiometer surface temperature patterns in the Santa Barbara Channel. *Journal of Geophysical Research* 93, 6863–6873.
- Large, W.G., Pond, S., 1981. Open ocean momentum flux measurements in moderate to strong winds. *Journal of Physical Oceanography* 11, 324–336.
- Lynn, R.J., Simpson, J.J., 1987. The California Current System: the seasonal variability of its physical characteristics. *Journal of Geophysical Research* 92, 12947–12966.
- Lynn, R.J., Baumgartner, T., Garcia, J., Collins, C.A., Hayward, T.L., Hyrenbach, K.D., Mantyla, A.W., Murphree, T., Shankle, A., Schwing, F.B., Sakuma, K.M., Tegner, M.J., 1998. The state of the California Current, 1997–1998: transition to El Niño conditions. *California Cooperative Oceanic Fisheries Investigations Reports* 31, 25–49.
- McClain, E.P., Pichel, W.G., Walton, C.C., 1985. Comparative performance of AVHRR-based multichannel sea surface temperatures. *Journal of Geophysical Research* 90, 11587–11601.
- Mertes, L.A.K., Warrick, J.A., 2001. Measuring flood output from 110 coastal watersheds in California with field measurements and SeaWiFS. *Geology* 29, 659–662.
- Mertes, L.A.K., Hickman, M., Waltenberger, B., Bortman, A.L., Inlander, E., McKenzie, C., Dvorsky, J., 1998. Synoptic views of sediment plumes and coastal geography of the Santa Barbara Channel, California. *Hydrological Processes* 12, 967–979.
- Milliman, J.D., Syvitski, J.P.M., 1992. Geomorphic/tectonic control of sediment discharge to the ocean: the importance of small mountainous rivers. *Journal of Geology* 100, 525–544.
- Mitchell, B.G., Kahru, M., 1998. Algorithms for SeaWiFS standard products developed with the CalCOFI bio-optical data set. *California Cooperative Oceanic Fisheries Investigations Report* 39, 133–147.
- Oey, L.-Y., Wang, D.-P., Hayward, T., Winant, C., Hendershott, M., 2001. Upwelling and cyclonic regimes of the near-surface circulation in the Santa Barbara Channel. *Journal of Geophysical Research* 106, 9213–9222.
- O'Reilly, J.E., Maritorena, S., Mitchell, B.G., Siegel, D.A., Carder, K.L., Garver, S.A., Kahru, M., McClain, C., 1998. Ocean color chlorophyll algorithms for SeaWiFS. *Journal of Geophysical Research* 103, 24,937–24,953.
- Otero, M.P., 2002. Spatial and temporal characteristics of sediment plumes and phytoplankton blooms in the Santa Barbara Channel. M.S. Thesis, University of California, Santa Barbara, unpublished.
- Reid Jr., J.L., Roden, G.I., Wyllie, J.G., 1958. Studies of the California Current System. *California Cooperative Oceanic*

- Fisheries Investigations Progress Report, 7-1-56 to 1-1-58, Marine Resources Committee, California Department of Fish and Game, Sacramento, CA, 27–56.
- Schwing, F.B., Moore, C.S., Ralston, S., Sakuma, K.M., 2000. Record coastal upwelling in the California Current in 1999. California Cooperative Oceanic Fisheries Investigations Reports 41, 148–160.
- Scott, K.M., Williams, R.P., 1978. Erosion and sediment yields in the Transverse Ranges, Southern California. United States Geological Survey Professional Paper 1030, 37pp.
- Shipe, R.F., Passow, U., Brzezinski, M.A., Siegel, D.A., Alldredge, A.L., 2002. Effects of the 1997–98 El Niño on seasonal variations in suspended and sinking particles in the Santa Barbara Basin. *Progress in Oceanography* 54, 105–127.
- Smith, R.C., Zhang, X., Michaelsen, J., 1998. Variability of pigment biomass in the California Current System as determined by satellite imagery. Part I: spatial variability. *Journal of Geophysical Research* 93, 10,863–10,882.
- Toole, D.A., Siegel, D.A., 2001. Modes and mechanisms of ocean color variability in the Santa Barbara Channel. *Journal of Geophysical Research* 106, 26985–27000.
- Toole, D.A., Siegel, D.A., Menzies, D.W., Neumann, M.J., Smith, R.C., 2000. Remote-sensing reflectance determinations in the coastal ocean environment: impact of instrumental characteristics and environmental variability. *Applied Optics* 39, 456–469.
- Venrick, E.L., 1998. The phytoplankton of the Santa Barbara Basin: patterns of chlorophyll and species structure and their relationships with those of surrounding stations. California Cooperative Oceanic Fisheries Investigations Reports 39, 124–132.
- Warrick, J.A., 2002. Short-term (1997–2000) and long-term (1928–2000) observations of river water and sediment discharge to the Santa Barbara Channel, California. PhD Dissertation, University of California, Santa Barbara.
- Warrick, J., Mertes, L.A.K., Washburn, L., Siegel, D.A., 2004. Dispersal forcing of southern California river plumes, based on field and remote sensing observations. *Geo-Marine Letters* 24, 46–52.
- Winant, C.D., Dorman, C.E., 1997. Seasonal patterns of surface wind stress and heat flux over the Southern California Bight. *Journal of Geophysical Research* 102, 5641–5653.
- Winant, C.D., Dever, E.P., Hendershott, M.C., 2003. Characteristic patterns of shelf circulation at the boundary between central and southern California. *Journal of Geophysical Research* 108 (C2), 3021.